Fall 2017

Natural Convection Heat Transfer of Inclined Sierpinski Carpet Fractal Fins

Luke A. Fussell

NATURAL CONVECTION HEAT TRANSFER FROM INCLINED SIERPINSKI CARPET FRACTAL FINS

by

LUKE FUSSELL

(Under the Direction of David Calamas)

ABSTRACT

When designing extended surfaces for the thermal management of electronic devices in aerospace applications it is critically important to minimize mass. However, this can be difficult to achieve as the rate of heat dissipated is directly proportional to the surface area. Fortunately, when certain fractal geometries, like the Sierpinski carpet, are utilized in the design of extended surfaces an increase in surface area and simultaneous decrease in mass can be achieved. The thermal performance of fins inspired by the first four fractal iterations of the Sierpinski carpet pattern was experimentally examined in a natural convection environment. The fractal fins were subject to a heat transfer rate of 10 W at their base and performance was evaluated for six different angles of inclination from 15° to 90°. The thermal performance of the fractal fins was evaluated based on fin efficiency, fin effectiveness, and fin effectiveness per unit mass. It was found that the angle of inclination did not have a statistically significant impact on performance. Regardless of angle of inclination, a fin inspired by the fourth fractal iteration was, on average, 6.1% more effective and 58.8% more effective per unit mass than a traditional straight rectangular fin of uniform cross-section.

INDEX WORDS: Thesis, Fractal, Sierpinski Carpet, Natural convection, Heat transfer, College of Graduate Studies, Georgia Southern University

NATURAL CONVECTION HEAT TRANSFER FROM INCLINED SIERPINSKI CARPET FRACTAL FINS

by

LUKE FUSSELL

B.S., Georgia Southern University, 2015

A Thesis Submitted to the Graduate Faculty of Georgia Southern University in

Partial Fulfillment of the Requirements for the Degree

MASTER OF SCIENCE

STATESBORO, GEORGIA

NATURAL CONVECTION HEAT TRANSFER FROM INCLINED SIERPINSKI CARPET FRACTAL FINS

by

LUKE FUSSELL

Major Professor:	David Calamas
Committee:	Marcel Ilie
	Biswanath Samanta

Electronic Version Approved:

December 2017

DEDICATION

To my family for always pushing me toward my goals.

ACKNOWLEDGMENTS

I would like to thank Dr. Calamas for giving me the opportunity to work on this research, and for constantly guiding me and teaching me along the way. I would also like to thank my fellow graduate students, Jacob Mayfield and Christopher Nutter, for discussing research ideas with me and helping me with experimental setups.

TABLE OF CONTENTS

Page

LIST OF TABLES

LIST OF FIGURES

INTRODUCTION

Background

Fins, or extended surfaces, are used to passively dissipate heat from a surface. It is critically important to dissipate waste heat from electronic devices in order to improve reliability and prevent premature failure of system components. When designing extended surfaces for the thermal management of electronic devices in aerospace applications it is critically important to minimize mass. However, this can be difficult to achieve as the rate of heat dissipated is directly proportional to the surface area. Fortunately, when certain fractal geometries, like the Sierpinski carpet, are utilized in the design of extended surfaces an increase in surface area and simultaneous decrease in mass can be achieved.

Motivation

The thermal performance of fins inspired by the Sierpinski carpet fractal pattern has been examined in natural and forced convection environments as well as in free space. However, in a natural convection environment, the orientation of the fins relative to the direction of gravity can impact performance. The effect of orientation, or angle of inclination, on the effectiveness of fractal fins has not yet been examined in a natural convection environment.

Objectives

The objective of this work is to: (1) experimentally investigate the thermal performance of the first four fractal iterations of the Sierpinski carpet pattern in a natural convection environment, (2) experimentally investigate the impact of orientation on fin efficiency and fin effectiveness for a range of angle of inclinations from 15^{o} to 90^{o} in increments of 15° relative to the direction of

gravity, and (3) assess if a fin inspired by the fourth fractal iteration of the Sierpinski carpet fractal pattern is more effective than the zeroth iteration, regardless of orientation.

Literature Review

The removal of waste heat generated by electronic devices is an essential task to ensure optimal performance and to reduce the risk of component failures. Often, extended surfaces, or fins, in the form of heat sinks are attached to surfaces where the excess heat must be dissipated from in an effort to provide an increase in surface area. Extended surfaces, or fins, are passive thermal management devices as they do not have any moving components. Heat sinks are often used in natural convection environments. Although the presence of extended surfaces result in an increase in heat transfer area, they often also result in an increase in mass. An increase in mass is undesirable in aerospace applications due to the high cost of sending mass into orbit. Fortunately, when certain fractal geometries are used in the design of fins or heat sinks the surface area available for heat transfer can be increased while system mass can be simultaneously decreased. This is the case for fins inspired by the Sierpinski carpet fractal pattern.

Mandelbrot describes fractals as a series of irregularities that are identical at any scale [1]. This is known as self-similarity. While literature in regard to the use of fractal perforations is somewhat limited, there is a large body of literature pertaining to the use of uniform square perforations. Al-Essa and Al-Hussein [2] numerically investigated the effect of orientation of square perforations on the rate of heat transfer. The authors found that it was better to orient the perforations parallel to the fin base rather than at an angle of inclination. Shaeri et al. [3] computationally investigated conjugate heat transfer from an array of rectangular fins with square perforations. The perforations in the rectangular fins were located parallel to the flow direction. Shaeri et al. concluded that for a Reynolds number range of 2000 to 5000 fins with perforations

had lower average friction coefficients when compared with solid fins. In addition, as the number of perforations increased fin efficiency was found to decrease due to a larger temperature difference between the base and tip of the fins. Shaeri and Yaghoubi [4] computationally investigated conjugate heat transfer from an array of rectangular fins with square perforations located perpendicular to the flow direction. Shaeri and Yaghoubi found for low Reynolds numbers the perforated fins offered similar performance as solid fins. However, for higher Reynolds numbers, perforated fins resulted in a significant increase in heat transfer. As the number of perforations increased so did the heat transfer enhancement. Shaeri and Jen [5] computationally examined the effects of size and number of perforations on the thermal performance of a rectangular fin array. As in Shaeri and Yaghoubi [4] the perforations were located perpendicular to the flow direction. Shaeri and Jen found for the same porosity fins with a smaller number of perforations were more efficient than fins with a larger number of perforations. Thus, for the same porosity, fins with larger perforations offer the greatest heat transfer enhancement.

Several authors have investigated the performance of extended surfaces with fractal perforations. Dannelley and Baker [6] experimentally investigated the use of fractal geometries to enhance the thermal performance of extended surfaces used for passive thermal management and concluded the effectiveness of the fractal fins was proportional to the surface area available for heat transfer. Dannelley and Baker concluded the effectiveness of extended surfaces with a Sierpinski carpet fractal pattern offered greater effectiveness per unit mass when compared with traditionally utilized straight rectangular fins. Dannelley and Baker experimentally tested the first three fractal iterations of the Sierpinski carpet pattern and hypothesized that a fourth iteration of the Sierpinski carpet fractal pattern would result in improved performance but were unable to experimentally verify their hypothesis due to fabrication constraints. In addition, Dannelley and

Baker isolated natural convection heat transfer in their calculations and thus did not comment on the impact of thermal radiation heat transfer. Dannelley and Baker [7] computationally investigated the use of fractal geometries to enhance the thermal performance of extended surfaces dissipating waste heat by natural convection alone and found a fourth iteration of the Sierpinski carpet fractal pattern can sufficiently improve fin effectiveness and effectiveness per unit mass when compared with traditionally employed straight rectangular fins. Dannelley and Baker studied Sierpinski carpet fractal fins of various width-to-thickness ratios and concluded that fin effectiveness was inversely proportional to width-to-thickness ratio. Dannelley and Baker [8] computationally investigated the use of fractal geometries to enhance the thermal performance of extended surfaces dissipating waste heat by thermal radiation to free space and found fin effectiveness per unit mass increased with fractal iteration for the Sierpinski carpet fractal pattern despite decreases in fin effectiveness and fin efficiency. Dannelley and Baker also developed a correlation for the effectiveness of Sierpinski carpet fractal fins radiating to free space for surface emissivities greater than or equal to 0.8. Calamas et al. [9] experimentally examined the thermal performance of fins inspired by the first four fractal iterations of the Sierpinski carpet pattern in a natural convection environment. Calamas et al. found that the fourth fractal iteration resulted in an increase in fin effectiveness and fin effectiveness per unit mass as hypothesized by Dannelley and Baker [6]. In addition, Calamas et al. found that thermal radiation accounted for a significant portion of the total rate of heat transfer and should not be neglected.

The use of fractal designs to enhance heat transfer is not limited to passive thermal management applications. Fractal designs have also been utilized in the design of heat exchangers. For example, Myer and Van Der Vyver [10] and Van Der Vyver et al. [11] analytically examined the performance of a double-pipe heat exchanger with a cross-section in accordance with the Koch

island fractal pattern. When compared with a traditional double-pipe heat exchanger, the use of the fractal pattern resulted in a significant increase in heat transfer area per unit volume.

Thermal radiation heat transfer, while often neglected in natural convection studies, can account for a significant percentage of the total heat transfer. The inclusion of thermal radiation in the design of fins and heat sinks can often affect a noticeable decrease in the size of a heat sink [12]. Yu et al. [13] experimentally and numerically investigated a radial heat sink and considered both natural convection and radiation in their analysis. Thermal radiation contributed up to 27% of the total heat transfer. Azarkish et al. [14] investigated the geometric optimization of a longitudinal fin with volumetric heat generation and found that the contribution of thermal radiation heat transfer, even for small values of surface emissivities, was large and should not be neglected.

There have been a limited number of publications in regard to the effect of angle of inclination on the thermal performance of perforated fins. Awasarmol and Pise [15] experimentally examined the performance of a perforated heat sink and found that the greatest heat transfer enhancement was achieved with larger perforations and at an orientation of 45° relative to the direction of gravity. Shen et al. [16] computationally investigated the performance of rectangular heat sinks as a function of orientation relative to the direction of gravity. The authors found that the closer packed, or denser, the fins in the heat sink are spaced, the greater the effect that orientation has on performance. The authors also found that flow blockage, due to the presence of neighboring fins, significantly impacted the thermal performance of the heat sinks. Upon summarizing the literature it is evident that the use of perforations results in an increase in thermal performance. In addition, the orientation of the fins also impacts performance. What has not been investigated is the use of fractal perforations at different angles of inclination.

Sierpinski Carpet Fractal Fins

The structure of the Sierpinski carpet fractal pattern begins with a square. The initial square, or zeroth fractal iteration, is composed of nine congruent squares each with a width one-third smaller than that of the previous fractal iteration. The central square is removed completing the first fractal iteration. After the central square is removed the previous procedure is applied recursively to the remaining squares until the desired fractal iteration is achieved. The first four iterations of the Sierpinski carpet fractal pattern can be seen in Figure 1. Prior studies oriented the fractal fins parallel to the direction of gravity. In this work, the orientation of the fractal fins will be varied. The nomenclature for the orientation of the fractal fins can be seen in Figure 2.

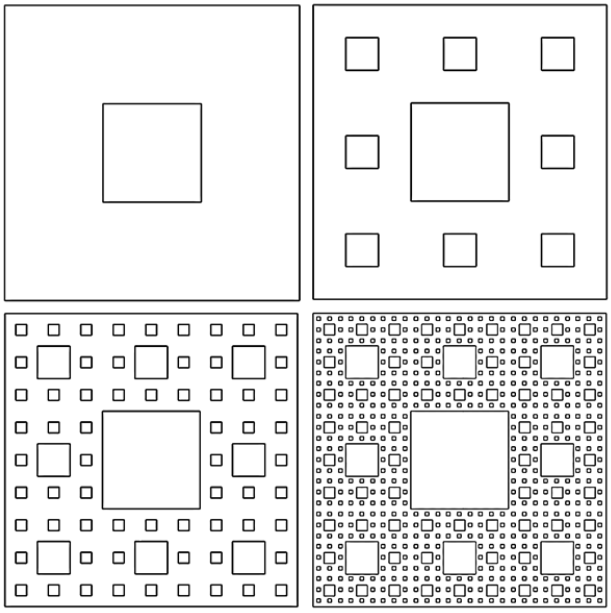

Figure 1 Sierpinski Carpet Fractal Iterations One through Four

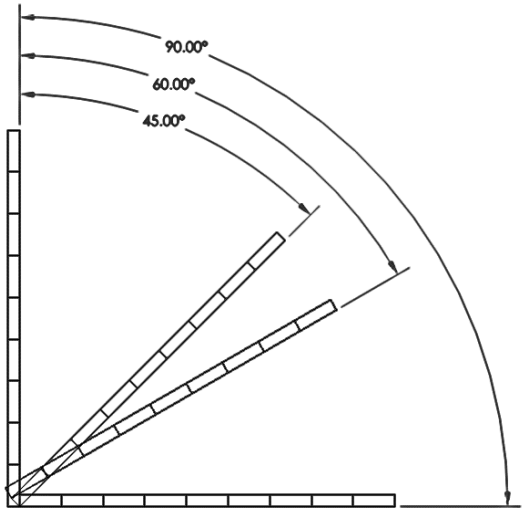

Figure 2 Nomenclature for Fin Orientation

The mass of a Sierpinski carpet extended surface is dependent on fractal iteration alone and can be found using Equation 1. The surface area of a Sierpinski carpet extended surface, also dependent on fractal iteration, can be found using Equation 2.

$$m(n) = \left[w^2 - \sum_{1}^{n} 8^{n-1}\left(\frac{w}{3^n}\right)^2\right]\rho t \qquad \text{Equation 1}$$

$$A_s(n) = 2w^2 + 3wt - \sum_{1}^{n} 8^{n-1}\left[2\left(\frac{w}{3^n}\right)^2 - 4\left(\frac{w}{3^n}\right)t\right] \qquad \text{Equation 2}$$

Due to the perforations associated with the fractal pattern, there is a reduction in mass with each fractal iteration as seen in Figure 3.

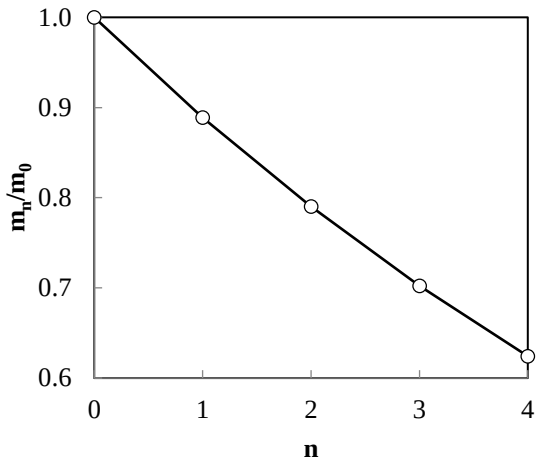

Figure 3 Mass Ratio as a Function of Fractal Iteration

The surface area of fins inspired by the Sierpinski carpet fractal pattern is a function of fractal iteration and the width-to-thickness ratio of the fins. The Sierpinski carpet fractal iterations in this experimental investigation have a width-to-thickness ratio of 32. The dimensionless surface area ratio as a function of fractal iteration can be seen in Figure 4. The purpose of utilizing a surface area ratio is that an increase or decrease in surface area when compared with the zeroth iteration can be readily identified. The zeroth iteration is a traditional straight rectangular fin of uniform cross-section and without perforations.

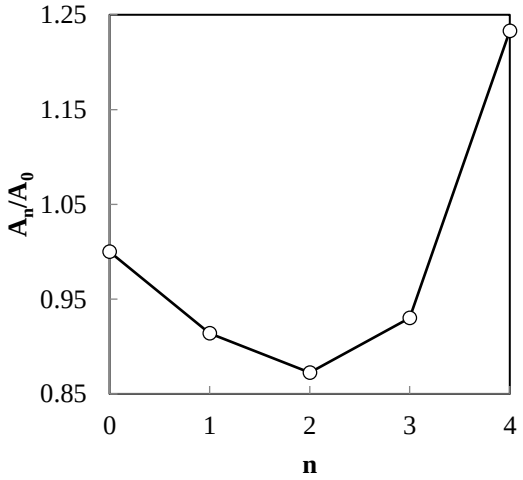

Figure 4 Surface Area of Sierpinski Fins as a Function of Fractal Iteration

The fin inspired by the fourth fractal iteration has a 23.65% increase in surface area when compared to the zeroth iteration while the first three iterations have a surface area less than that of the zeroth iteration. From this it can be predicted that additional iterations would results in an exponential increase in surface area.

The fractal fins were manufactured out of Aluminum 5052-H32. Each fractal fin has a final width and height of 5.08 cm (2 in) and a thickness of 1.5875 mm (1/16 in). The fractal fins were sandblasted and anodized with a matte black surface finish to achieve a surface emissivity of 0.99. The mass and surface area of the Sierpinski carpet fractal fins utilized in the experimental analysis can be seen in Table 1.

Table 1 Sierpinski Carpet Fin Mass and Surface Area

n	As (cm^2)	m (g)
0	53.23	10.98
1	48.57	9.76
2	46.34	8.68
3	49.45	7.71
4	65.81	6.85

CHAPTER 1: NATURAL CONVECTION HEAT TRANSFER OF INCLINED SIERPINSKI CARPET FRACTAL FINS

Introduction

Natural convection heat transfer on an extended surface, or fin, depends on the geometry of the surface as well as its orientation. While, the thermal performance of fins inspired by the Sierpinski carpet fractal pattern have been investigated in a natural convection environment, the fins were only oriented parallel to the direction of gravity. In the following section, the impact that the angle of inclination has on the effectiveness and efficiency of the fractal fins will be examined.

Experimental Methodology

The fractal fins, corresponding to the first four iterations of the Sierpinski carpet fractal pattern, can be seen in Figure 5.

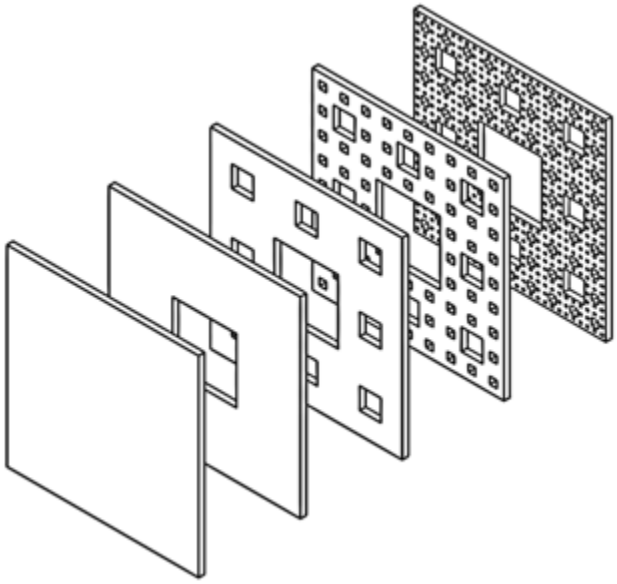

Figure 5 Sierpinski Carpet Fractal Fins Iterations Zero through Four

A heat transfer rate was applied to the base of the fin for testing using a Kapton® flexible thin film insulated heater that was adhered to the fin using a pressure-sensitive adhesive (Omega® KHLV-104/2-P). The area of the fin that had the heat transfer rate applied was surrounded by Techlite® melamine foam insulation ($k = 0.036\ W/m{\cdot}K$) to reduce the amount of heat loss. A power supply was used to set the heat transfer rate to the thin film heater (B&K Precision 9130). Omega Type T thermocouples (Omega TMQSS-125U-6) were used to measure the ambient temperature as well as the surface temperature of the flexible thin film heaters. In addition the thermocouples were used to measure the loss through the insulation at three different locations. The thermocouples were placed in the insulation 1.27 cm (0.5 in) from the back of the fin, 1.27 cm (0.5 in) from the side of the fin, and 1.27 cm (0.5 in) below the fin. In addition, a Type T surface thermocouple was adhesively placed on the surface of the fin to measure the temperature of the fin's base. A temperature controller (Omega® CSC32) was used in series with the power supply to prevent the flexible thin film heater from exceeding the flash point of the melamine foam insulation. An Omega® Type K thermocouple, connected to the benchtop temperature controller, was used to monitor the temperature of the film heater and shut off the power supply if the temperature at the base of the fin exceeded 170°C (the Techlite® melamine foam has a flashpoint of 176°C). A 16 channel thermocouple compact data acquisition (DAQ) module (National Instruments 9213) and chassis (National Instruments cDAQ-9171) was used in conjunction with National Instruments LabVIEW software to monitor the temperature of all 5 thermocouples. A FLIR® A325sc infrared camera was used to monitor the temperature profile of the fin during experiments. The infrared camera was used to calculate the average base temperature and average tip temperature of the fin using a line average. The surface temperature of the fin was assumed to be the average of the base temperature and tip temperature as measured by the infrared camera.

Final temperatures were recorded after steady-state temperatures were achieved. Due to noise from the environment, a black hardboard was placed behind the experimental setup to ensure accurate readings from the infrared camera. The experimental layout can be seen in Figure 6.

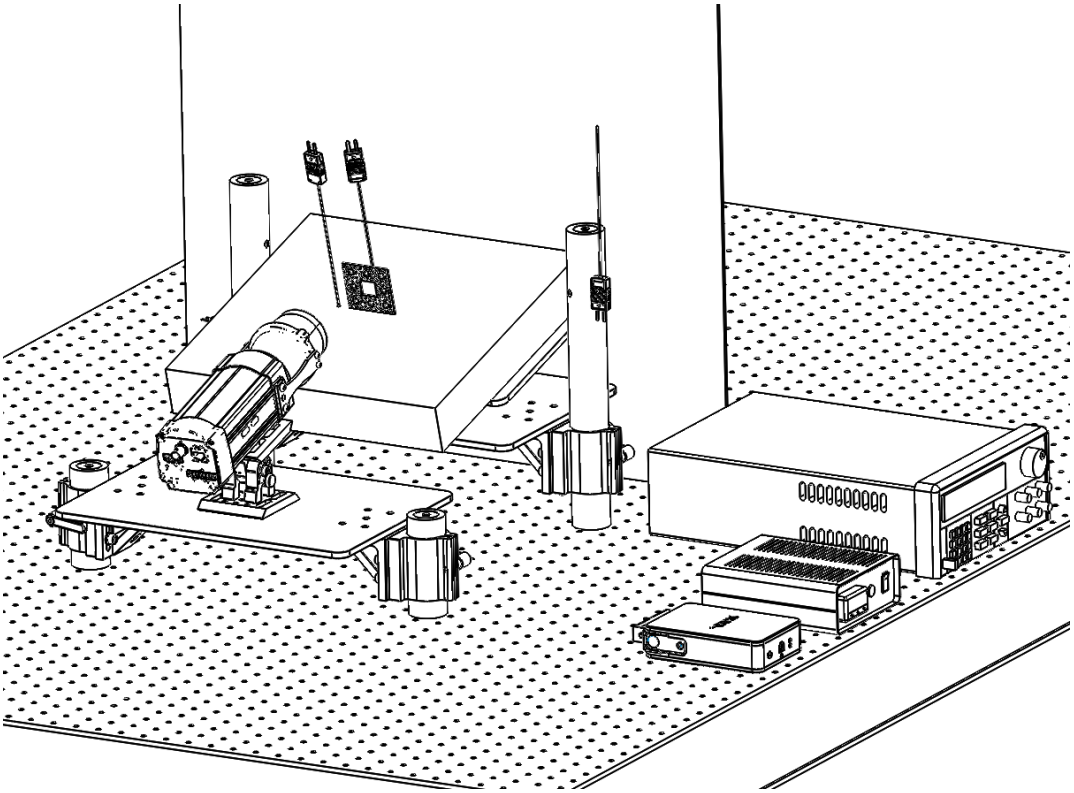

Figure 6 Sierpinski Carpet Experimental Layout

Two adjustable angle mounts were utilized to control the angle of the camera and the surface of the fin. The two angle mounts allowed the infrared camera to always image directly normal to the heated fin surface. The adjustable angle amounts allowed the fins to be orientated at different angles with respect to gravity. In this analysis, six different angles of inclination were investigated: 15, 30, 45, 60, 75 and 90°. Fins inspired by the first four iterations of the Sierpinski carpet fractal pattern, subject to 10 W of power input at their base, were experimentally examined for each of the aforementioned orientations.

Results

Experimental Calculations

During this experimental study each fractal fin was subject to 10 W of heat applied at the base via the flexible thin film heaters. The power supplied is a product of the voltage and current applied by the power supply. The amount of heat loss via conduction through the insulation was calculated in accordance with Fourier's Law as shown in Equation 3.

$$\dot{Q}_{loss} = \sum \left(-kA_s \frac{\partial T}{\partial n} \right) \quad \text{Equation 3}$$

In order to calculate the magnitude of convective heat transfer, the magnitude of radiative heat transfer, in addition to loss through the insulation, must be known (see Equation 4 and Equation 5). The ambient temperature, measured by a thermocouple, and the average surface temperature as measured by the infrared camera, were used to calculate the heat dissipated by the fin via thermal radiation

$$\dot{Q}_{rad} = \varepsilon \sigma F_n A_s (T_s^4 - T_{amb}^4) \quad \text{Equation 4}$$

$$\dot{Q}_{conv} = P - \dot{Q}_{loss} - \dot{Q}_{rad} \quad \text{Equation 5}$$

In order to calculate the rate of radiative heat transfer, an average view factor for each of the fractal fins was calculated. This was done by first calculating the view factor for each of the different perforation sizes. The view factor for each of the square perforations was calculated in accordance with a view factor correlation for perpendicular rectangles with a common edge. Each perforation size had a different view factor, and a fin inspired by the fourth iteration of the Sierpinski carpet fractal pattern has four different perforation sizes. To account for the different perforations sizes (and thus view factors) an area weighting term, corresponding to each fractal iteration, was utilized. The area weighting term indicated the percentage of the total surface area the perforations

accounted for. The average view factor for each fin, shown in Table 2, indicates the percentage of heat transfer emitted by the surfaces that was exchanged with the surroundings. Each perforated fractal fin has a view factor less than unity due to intersurface thermal radiation within the perforations.

Table 2 Average View Factor Coefficients for Fractal Iterations

n	Average Fin View Factor(F_n)
0	1.0000
1	0.9972
2	0.9797
3	0.8966
4	0.6737

Once the rate of convective heat transfer was determined, the average heat transfer coefficient was then calculated using Equation 6 below.

$$h = \frac{\dot{Q}_{conv}}{A_s(T_s - T_{amb})} \qquad \text{Equation 6}$$

The two primary performance metrics used when evaluated the thermal performance of extended surfaces are fin efficiency and fin effectiveness. Fin effectiveness (Equation 7) is the ratio of the actual heat transfer rate from the fin to the heat transfer rate from the base area in the absence of the fin. Fin efficiency (Equation 8) is the ratio of the actual heat transfer rate from the fin to the ideal heat transfer rate from the fin if the entire fin were at the base temperature.

$$\varepsilon_{fin} = \frac{\dot{Q}_{conv}}{hA_b(T_{base} - T_{amb})} \qquad \text{Equation 7}$$

$$\eta = \frac{\dot{Q}_{conv}}{hA_s(T_{base} - T_{amb})} \qquad \text{Equation 8}$$

Data

A total of 150 experimental trials were carried out. Each of the five fins, corresponding to fractal iterations zero through four, were experimentally tested five times. Each of the aforementioned fractal fins was also examined for each of the six angles of inclination (from 15 to 90°) .The results of each trial can be seen in Table 3 and Table 4 which show the two primary performance metrics – fin efficiency and fin effectiveness.

Table 3 Fin Performance Results for Trials at Angles 15, 30, and 45

Angle	15 Degrees			30 Degrees			45 Degrees		
Iteration	η	ε	ε/m_n (kg^{-1})	η	ε	ε/m_n (kg^{-1})	η	ε	ε/m_n (kg^{-1})
0	0.91	60.26	5488.04	0.91	60.27	5489.47	0.91	59.85	5450.77
	0.91	60.08	5472.49	0.91	60.34	5495.79	0.91	60.02	5466.47
	0.91	60.38	5498.99	0.91	60.31	5493.03	0.91	60.12	5475.73
	0.92	60.48	5508.86	0.92	60.46	5506.40	0.91	59.98	5463.41
	0.92	60.42	5503.09	0.91	60.38	5499.25	0.91	60.32	5493.76
1	0.90	54.11	5544.63	0.89	53.51	5482.54	0.90	54.12	5544.95
	0.90	54.23	5557.06	0.90	53.92	5525.14	0.89	53.83	5515.92
	0.90	54.43	5576.98	0.89	53.76	5508.86	0.89	53.72	5504.59
	0.90	54.07	5540.79	0.89	53.89	5521.39	0.89	53.77	5509.42
	0.90	54.12	5545.28	0.89	53.63	5495.47	0.90	53.93	5525.82
2	0.88	50.49	5820.72	0.87	50.19	5785.28	0.87	49.88	5749.43
	0.88	50.44	5813.95	0.87	50.12	5777.24	0.87	49.96	5759.55
	0.88	50.38	5807.97	0.87	50.22	5788.90	0.87	49.80	5740.58
	0.88	50.40	5809.97	0.87	50.22	5788.50	0.87	49.75	5734.47
	0.87	50.13	5778.21	0.87	50.13	5778.59	0.87	49.97	5760.70
3	0.83	50.80	6588.22	0.84	51.81	6718.72	0.84	51.40	6665.38
	0.83	50.81	6588.54	0.84	51.72	6707.12	0.84	51.43	6670.18
	0.83	50.77	6584.54	0.84	51.47	6674.21	0.84	51.51	6680.54
	0.83	50.84	6593.40	0.84	51.30	6652.52	0.84	51.55	6684.87
	0.83	50.92	6603.99	0.85	51.95	6737.24	0.84	51.61	6692.78
4	0.80	65.14	9503.98	0.79	64.39	9393.83	0.77	62.78	9158.83
	0.80	65.34	9533.27	0.79	64.34	9386.23	0.77	62.79	9160.59
	0.80	65.59	9569.06	0.79	64.32	9384.12	0.78	63.26	9229.46
	0.80	65.22	9515.50	0.79	64.55	9417.86	0.78	63.65	9286.27
	0.80	64.97	9478.40	0.80	65.20	9511.99	0.77	63.11	9207.77

Table 4 Fin Performance Results for Trials at Angles 60, 75, and 90

Angle	60 Degrees			75 Degrees			90 Degrees		
Iteration	η	ε	ε/m_n (kg^{-1})	η	ε	ε/m_n (kg^{-1})	η	ε	ε/m_n (kg^{-1})
0	0.90	59.58	5426.60	0.91	59.98	5463.14	0.91	60.37	5498.48
	0.90	59.58	5426.60	0.91	60.07	5471.59	0.91	60.20	5482.90
	0.90	59.67	5435.04	0.91	60.32	5493.60	0.92	60.42	5502.85
	0.90	59.68	5435.54	0.91	60.22	5484.55	0.91	60.17	5480.25
	0.91	59.89	5454.40	0.91	60.25	5487.39	0.91	59.91	5456.48
1	0.88	53.21	5452.63	0.89	53.73	5505.69	0.89	53.49	5480.75
	0.89	53.36	5467.30	0.89	53.63	5495.32	0.89	53.58	5490.43
	0.89	53.50	5481.80	0.89	53.61	5493.34	0.89	53.54	5485.59
	0.89	53.41	5472.95	0.89	53.86	5519.07	0.89	53.59	5491.30
	0.89	53.86	5519.19	0.89	53.74	5506.37	0.89	53.32	5463.42
2	0.86	49.55	5711.77	0.85	48.91	5638.13	0.86	49.68	5727.31
	0.87	49.92	5753.96	0.86	49.21	5672.56	0.87	49.90	5752.19
	0.87	49.80	5740.36	0.86	49.50	5706.48	0.87	50.03	5767.15
	0.86	49.64	5722.40	0.87	49.91	5753.50	0.87	49.71	5729.94
	0.87	49.72	5731.72	0.87	49.72	5731.20	0.87	49.91	5753.50
3	0.82	50.23	6513.58	0.83	51.01	6614.54	0.83	50.80	6587.68
	0.82	50.34	6528.41	0.83	50.75	6581.67	0.83	51.03	6617.17
	0.82	50.43	6539.93	0.83	51.19	6638.79	0.83	50.73	6578.39
	0.82	50.30	6522.83	0.83	50.88	6597.72	0.83	50.82	6590.29
	0.82	50.27	6518.91	0.83	50.86	6595.41	0.82	50.19	6508.37
4	0.77	62.76	9155.96	0.78	63.88	9319.03	0.78	63.70	9293.54
	0.77	62.50	9118.66	0.78	63.60	9278.99	0.78	63.84	9314.02
	0.76	62.22	9077.75	0.78	63.51	9266.21	0.78	63.38	9246.76
	0.77	63.12	9209.02	0.78	63.54	9270.04	0.77	63.10	9205.57
	0.77	62.85	9169.65	0.78	63.75	9300.46	0.78	63.32	9237.99

Statistical Analysis

A statistical analysis was performed to account for random errors in the experiment. A 95% confidence level was utilized in the statistical analysis. Data collected for the statistical analysis can be seen in Table 5 and Table 6.

Table 5 Average Fin Performance Metrics at Angles 15, 30, and 45

		η			ε			ε/m_n (kg^{-1})		
Angle	n	Avg.	Std.	C.I. ±	Avg.	Std.	C.I. ±	Avg.	Std.	C.I. ±
15°	0	0.91	0.002	0.003	60.32	0.16	0.20	5494.29	14.37	17.84
	1	0.90	0.002	0.003	54.19	0.14	0.18	5552.95	14.75	18.31
	2	0.88	0.002	0.003	50.37	0.14	0.18	5806.16	16.37	20.33
	3	0.83	0.001	0.001	50.83	0.06	0.07	6591.74	7.54	9.36
	4	0.80	0.001	0.001	65.25	0.06	0.07	9520.04	7.54	9.36
30°	0	0.91	0.001	0.001	60.35	0.07	0.09	5496.79	6.47	8.03
	1	0.89	0.003	0.004	53.74	0.17	0.22	5506.68	17.82	22.13
	2	0.87	0.001	0.001	50.17	0.05	0.06	5783.70	5.49	6.81
	3	0.84	0.004	0.005	51.65	0.26	0.33	6697.96	34.23	42.50
	4	0.79	0.004	0.005	64.56	0.26	0.33	9418.81	34.23	42.50
45°	0	0.91	0.003	0.003	60.06	0.18	0.22	5470.03	15.99	19.86
	1	0.89	0.003	0.003	53.87	0.16	0.19	5520.14	15.99	19.85
	2	0.87	0.002	0.002	49.87	0.10	0.12	5748.95	11.51	14.30
	3	0.84	0.001	0.002	51.50	0.09	0.11	6678.75	11.06	13.74
	4	0.77	0.001	0.002	63.12	0.09	0.11	9208.58	11.06	13.74

Table 6 Average Fin Performance Metrics at Angles 60, 75, and 90

		η			ε			ε/m_n (kg^{-1})		
Angle	n	Avg.	Std.	C.I. ±	Avg.	Std.	C.I. ±	Avg.	Std.	C.I. ±
60°	0	0.90	0.002	0.002	59.68	0.12	0.15	5435.64	11.36	14.10
	1	0.89	0.004	0.005	53.47	0.24	0.30	5478.77	24.96	30.99
	2	0.87	0.002	0.003	49.73	0.14	0.17	5732.04	16.23	20.15
	3	0.82	0.001	0.002	50.31	0.08	0.10	6524.73	10.08	12.52
	4	0.77	0.001	0.002	62.69	0.08	0.10	9146.21	10.08	12.52
75°	0	0.91	0.002	0.003	60.17	0.14	0.17	5480.05	12.40	15.40
	1	0.89	0.002	0.002	53.72	0.10	0.12	5503.96	10.30	12.79
	2	0.86	0.007	0.009	49.45	0.40	0.50	5700.37	45.99	57.10
	3	0.83	0.003	0.003	50.94	0.17	0.21	6605.63	21.91	27.20
	4	0.78	0.003	0.003	63.66	0.17	0.21	9286.94	21.91	27.20
90°	0	0.91	0.003	0.004	60.21	0.20	0.25	5484.19	18.29	22.71
	1	0.89	0.002	0.002	53.50	0.11	0.14	5482.30	11.36	14.11
	2	0.87	0.003	0.003	49.85	0.15	0.18	5746.02	16.95	21.05
	3	0.83	0.005	0.006	50.71	0.31	0.39	6576.38	40.67	50.49
	4	0.78	0.005	0.006	63.47	0.31	0.39	9259.58	40.67	50.49

Experimental Uncertainty Analysis

An experimental uncertainty analysis was performed in order to account for all possible systematic that could have occurred during experimentation. The calculations performed for this analysis were found using $U_s = \left[\sum\left\{\left(\frac{\partial S}{\partial x_n}\right)U_{x_n}\right\}^2\right]^{\frac{1}{2}}$ Equation 9, which was presented by Wheeler and Ghanji [17].

$$U_s = \left[\sum\left\{\left(\frac{\partial S}{\partial x_n}\right)U_{x_n}\right\}^2\right]^{\frac{1}{2}} \quad \text{Equation 9}$$

Where U_s is the total experimental uncertainty, S is the metric that is being analyzed, x_n is a variable contained in the S equation. The measurement uncertainty of the infrared camera was 2℃. The measurement uncertainty for the thermocouples was 1℃. The measurement uncertainty for the voltage and current output from the bench top power supply was 0.01% + 3mV and 0.1% + 3mA respectively. The measurement uncertainty for the scale used to measure the mass of the fins was 0.1g. The measurement uncertainty of the digital micrometer used to measure the dimensions of the fins was 0.01mm. As an example, the equations utilized to address the propagation of uncertainty for the main performance metrics (fin efficiency, fin effectiveness, and fin effectiveness per unit mass) can be found below. The equations below show the expanded versions of $U_s = \left[\sum\left\{\left(\frac{\partial S}{\partial x_n}\right)U_{x_n}\right\}^2\right]^{\frac{1}{2}}$ Equation 9 for the three primary performance metrics of this experimental study.

$$U_\eta = \left[\left(\frac{\partial \eta}{\partial \dot{Q}_{conv}}U_{\dot{Q}_{conv}}\right)^2 + \left(\frac{\partial \eta}{\partial h}U_h\right)^2 + \left(\frac{\partial \eta}{\partial T_{base}}U_{T_{base}}\right)^2 + \left(\frac{\partial \eta}{\partial T_{amb}}U_{T_{amb}}\right)^2\right]^{\frac{1}{2}} \quad \text{Equation 10}$$

$$U_{\varepsilon_{fin}} = \left[\left(\frac{\partial \varepsilon_{fin}}{\partial \dot{Q}_{conv}}U_{\dot{Q}_{conv}}\right)^2 + \left(\frac{\partial \varepsilon_{fin}}{\partial h}U_h\right)^2 + \left(\frac{\partial \varepsilon_{fin}}{\partial T_{base}}U_{T_{base}}\right)^2 + \left(\frac{\partial \varepsilon_{fin}}{\partial T_{amb}}U_{T_{amb}}\right)^2\right]^{\frac{1}{2}} \quad \text{Equation 11}$$

$$U_{\varepsilon_{fin/m}} = \left[\left(\frac{\partial \varepsilon_{fin/m}}{\partial \varepsilon_{fin}} U_{\varepsilon_{fin}}\right)^2\right]^{\frac{1}{2}} \quad \text{Equation 12}$$

The experimental uncertainty results for the performance metrics calculated with the above three equations can be seen in Table 7.

Table 7 Average Experimental Uncertainty for All Trials

	U_η		U_ε		$U_{\varepsilon/mn\ (kg\text{-}1)}$	
n	Avg.	Std.	Avg.	Std.	Avg.	Std.
0	0.03	0.001	1.71	0.08	155.44	6.86
1	0.02	0.001	1.28	0.03	131.32	3.37
2	0.02	0.001	1.15	0.04	132.39	4.65
3	0.02	0.001	1.13	0.07	146.59	9.70
4	0.02	0.001	1.62	0.12	236.25	17.03

Discussion

In the following sections average values for the primary performance metrics are presented. The primary interest is the thermal performance of the fin inspired by the fourth fractal iteration. This is because the fourth iteration has a greater surface area when compared with the zeroth iteration. It should be noted that the zeroth iteration would correspond to a traditional straight rectangular fin of uniform cross-section and without perforations. Fin efficiency was found to decrease with fractal iteration, regardless of the orientation of the fractal fins as shown in Figure 7. The difference in fin efficiency between angles of inclination was within the bounds of the experimental uncertainty and is thus not significant. This is also true in regards to the statistical accuracy. The decrease in fin efficiency can largely be attributed to the reduction in the tip temperature of the fin

relative to the base temperature. A fin inspired by the fourth iteration of the Sierpinski carpet fractal pattern was, on average, 14.2% less efficient than the zeroth iteration (the baseline case).

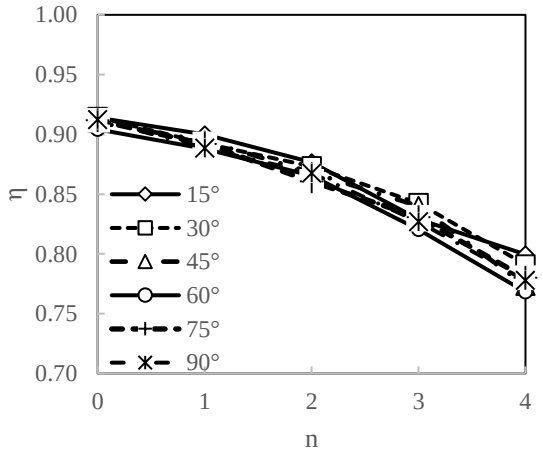

Figure 7 Fin Efficiency as a Function of Fractal Iteration and Angle

Fin effectiveness is arguably the more important performance metric as it shows the increase in the rate of heat transfer that the presence of a fin provides. The effectiveness follows a qualitatively similar trend as the surface area (see Figure 4) and can be seen in Figure 8. The fractal fin corresponding to fractal iteration four has a surface area 23.65% greater than that of the zeroth iteration. This increase in surface area results in an average increase in effectiveness of 6.1%.

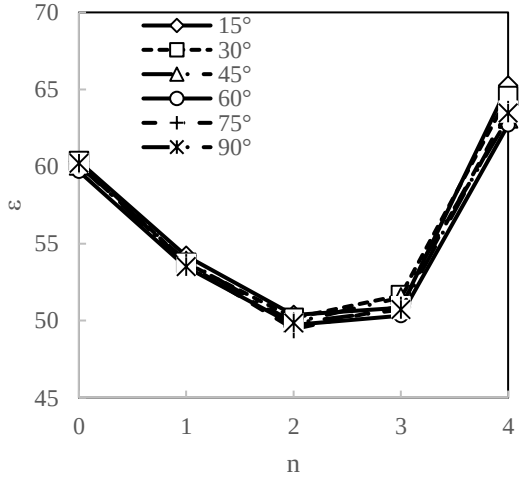

Figure 8 Convective Fin Effectiveness as a Function of Fractal Iteration and Angle

The increase in effectiveness follows an exponential trend and it is hypothesized that a fifth iteration would result in a greater increase in effectiveness. It should be noted that, pending the size of the fin, fabrication of a fifth iteration may be difficult and costly. While the convective effectiveness increases after the third iteration the radiative effectiveness does not as shown in Figure 9. This is because, as the number of iterations increases, so does the number of perforations. As the number of perforations increases, so does the amount of intersurface thermal radiation within the perforations. Thus, the more intersurface thermal radiation, the less radiative exchange with the surroundings.

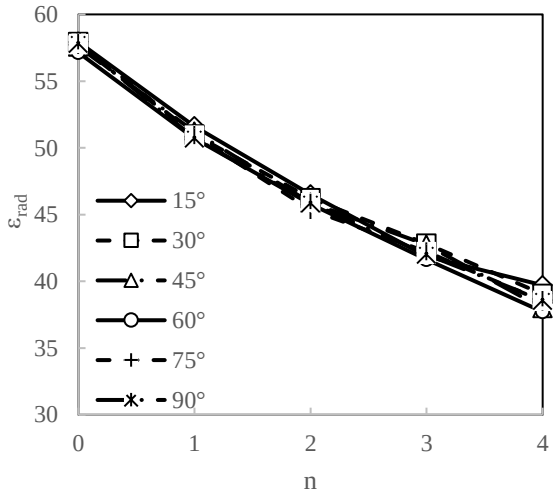

Figure 9 Radiative Fin Effectiveness as a Function of Fractal Iteration and Angle

The total effectiveness considers the radiative and convective effectiveness of the fin. Results of total effectiveness can be seen from the curve in Figure 10. The results of total effectiveness show a decrease in overall effectiveness compared to the convective effectiveness. However, it should be noted that the radiative effectiveness is largely a function of the width-to-thickness ratio of the fins. If the fractal fins were thinner then there would be less intersurface thermal radiation and the radiative and total effectiveness would increase.

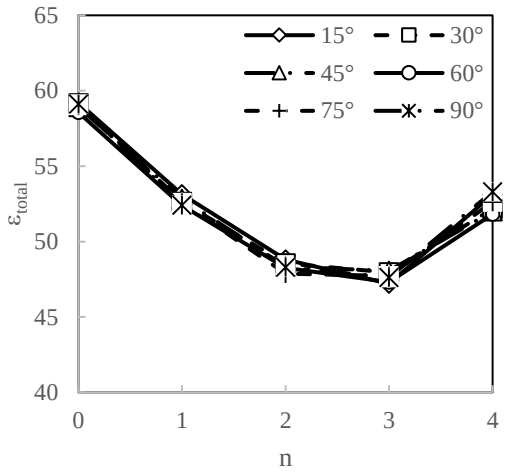

Figure 10 Total Fin Effectiveness as a Function of Fractal Iteration and Angle

As previously mentioned, in aerospace applications it is critical to maximize heat transfer while at the same time minimizing mass. To account for this, fin effectiveness per unit mass was determined and the results can be seen in Figure 11.

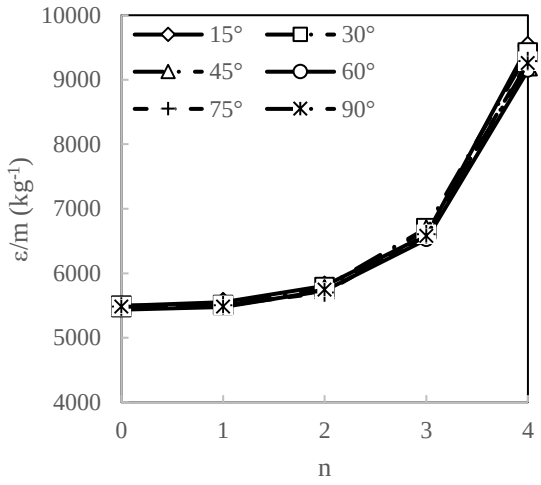

Figure 11 Fin Effectiveness per Unit Mass as a Function of Fractal Iteration and Angle

While the first three iterations result in a decrease in effectiveness, fin effectiveness per unit mass increases with each fractal iteration. The reduction in area associated with the first three iterations is offset by the exponential decrease in mass. In the case of the fourth iteration, which has a surface area 23.65% greater, and mass 37.6% less, than the zeroth iteration, there is a 69.9% increase in

fin effectiveness per unit mass. As with fin efficiency and fin effectiveness, the orientation of the fins relative to the direction of gravity did not impact fin effectiveness per unit mass. As a fin inspired by the fourth iteration is the most effective the fourth iteration was compared directly to the zeroth iteration which represents the baseline case of a traditional rectangular fin without perforations. The difference in performance between the fourth and zeroth iteration can be seen in

Table 8.

Table 8 Percent (%) Change from Fourth Iteration to Zeroth Iteration

Angle	η	ε	ε/m_n (kg^{-1})
15	-12.5%	8.2%	73.3%
30	-13.5%	7.0%	71.4%
45	-15.0%	5.1%	68.3%
60	-15.0%	5.0%	68.3%
75	-14.4%	5.8%	69.5%
90	-14.8%	5.4%	68.8%

As previously noted, thermal radiation accounts for an appreciable percentage of the total heat transfer rate. However, as the number of fractal iterations increases, the contribution of thermal radiation heat transfer decreases (Figure 12). This is due to the decrease in the average view factor of each of the fins. As the number of iterations increases, so does the magnitude of intersurface thermal radiation which results in a decrease in radiative heat transfer exchange with the surroundings. For example, fins inspired by the first three iterations of the Sierpinski carpet fractal pattern exchange 90% or greater of the radiation emitted with the surroundings. However, the fourth iteration only exchanges 67% of the radiation emitted with the surroundings (see Table 2).

It should be noted that only one angle of inclination is shown in the figure below as the other angles resulted in both qualitatively and quantitatively similar trends.

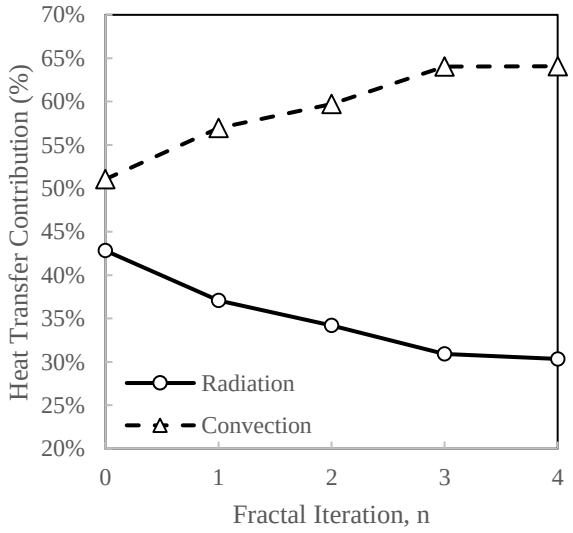

Figure 12 Heat Transfer Contribution for 75 degree angle as a function of fractal iteration

CONCLUSION

The thermal performance of fins inspired by the first four iterations of the Sierpinski carpet fractal pattern was experimentally examined in a natural convection environment. The fractal fins thermal performance was evaluated based on fin efficiency, fin effectiveness, and fin effectiveness per unit mass. The primary consideration in this study was the orientation of the fins. Six different angles of inclination, from 15° to 90° relative to the direction of gravity in increments of 15° were examined for each of the fractal fins. Results indicated that the orientation of the fins relative to gravity did not impact the thermal performance. The change in performance between each angle of inclination was within the bounds of the experimental uncertainty. Likewise, the change in performance did not prove to be statistically significant. In good agreement with prior research, a

fin inspired by the fourth iteration of the Sierpinski carpet fractal pattern was on average 6.1% more effective and 58.8% more effective per unit mass when compared with the zeroth iteration (a straight rectangular fin of uniform cross-section and without perforations). It is evident that a fin inspired by the fourth iteration is a robust design as performance did not degrade with orientation.

REFERENCES

[1] B. Mandelbrot, The Fractal Geometry of Nature, New York: W. H. Freeman, 1982.

[2] A. H. Al-Essa and F. M. Al-Hussien, "The Effect of Orientation of Square Perforations on the Heat Transfer Enhancement from a Fin Subjected to Natural Convection," *Heat and Mass Transfer,* vol. 40, no. 6-7, pp. 509-515, 2004.

[3] M. R. Shaeri, M. Yaghoubi and K. Jafarpur, "Heat Transfer Analysis of Lateral Perforated Fin Heat Sinks," *Journal of Applied Energy,* vol. 86, pp. 2019-2029, 2009.

[4] M. R. Shaeri and M. Yaghoubi, "Thermal Enhancement from Heat Sinks by Using Perforated Fins," *Journal of Energy Conversion and Management,* vol. 50, no. 5, pp. 1264-1270, 2009.

[5] M. R. Shaeri and T. C. Jen, "The Effects of Perforation Sizes on Laminar Heat Transfer Characteristics of an Array of Perforated Fins," *Journal of Energy Conversion and Management,* vol. 64, pp. 328-334, 2012.

[6] D. Dannelley and J. Baker, "Natural Convection Fin Performance Using Fractal-Like Geometries," *Journal of Thermophysics and Heat Transfer,* vol. 26, no. 4, pp. 657-664, 2012.

[7] D. Dannelley and J. Baker, "Natural Convection Heat Transfer from Fractal-Like Fins," *Journal of Thermophysics,* pp. 692-699, 2013.

[8] D. Dannelley and J. Baker, "Radiant Fin Performance Using Fractal-Like Geometries," *Journal of Heat Transfer,* vol. 135, no. 8, 2013.

[9] D. Calamas, D. Dannelley and G. Keten, "Experimental Effectieness of Sierpinski Carpet Fractal Fins in a Natural Convection Environment," *Journal of Heat Transfer,* 2017.

[10] J. P. Meyer and H. Van Der Vyver, "Heat Transfer Characteristics of a Quadratic Koch Island Fractal Heat Exchanger," *Heat Transfer Engineering,* vol. 26, no. 9, pp. 22-29, 2005.

[11] H. Van Der Vyver, J. Dirker and J. P. Meyer, "Validation of a CFD Model of a Three-Dimensional Tube-in-Tube Heat Exchanger," in *Third Indernational COnference on CFD in the Minerals and Process INdustries,* Melbourne, 2003.

[12] S. Rae and S. E. West, "Thermal Radiation from Finned Heat Sinks," *IEEE Transactions on Parts, Hybrids, and Packaging,* vol. 12, no. 2, pp. 115-117, 1976.

[13] S. H. Yu, D. Jang and K. S. Lee, "Effect of Radiation in a Radial Heat Sink Under Natural Convection," *International Journal of Heat and Mass Transfer,* vol. 55, pp. 505-509, 2012.

[14] H. Azarkish, S. M. Sarvari and A. Behzademehr, "Optimum Geometry of a Longitudinal Fin with Volumetric Heat Generation under the influences of Natural Convection and Radiation," *Journal of Energy Conversion and Management,* pp. 1938-1946, 2010.

[15] U. V. Awasarmol and A. T. Pise, "An Experimental Investigation of Natural Convection Heat Tranfser Enhancement from Perforated Rectangular Fin Array at Different Inclinations," *Experimental Thermal and Fluid Science,* vol. 68, pp. 145-154, 2015.

[16] Q. Shen, D. Sun, Y. Xu, T. Jin and X. Zhao, "Orientation Effects on Natural Convection Heat Dissipation of Rectangular FIn Heat Sinks Mounted on LEDs," *International Journal of Heat and Mass Transfer,* vol. 75, pp. 462-469, 2014.

[17] A. J. Wheeler and A. R. Ghanji, Introduction to Engineering Experimentation, Pearson, 2004.